CMS

CERN-PH-EP/2013-217
2014/05/20

CMS-SMP-12-011

Measurement of inclusive W and Z boson production cross sections in pp collisions at $\sqrt{s} = 8\,\text{TeV}$

The CMS Collaboration[*]

Abstract

A measurement of total and fiducial inclusive W and Z boson production cross sections in pp collisions at $\sqrt{s} = 8\,\text{TeV}$ is presented. Electron and muon final states are analyzed in a data sample collected with the CMS detector corresponding to an integrated luminosity of $18.2 \pm 0.5\,\text{pb}^{-1}$. The measured total inclusive cross sections times branching fractions are $\sigma(\text{pp} \rightarrow \text{W}X) \times \mathcal{B}(\text{W} \rightarrow \ell\nu) = 12.21 \pm 0.03\,(\text{stat.}) \pm 0.24\,(\text{syst.}) \pm 0.32\,(\text{lum.})\,\text{nb}$ and $\sigma(\text{pp} \rightarrow \text{Z}X) \times \mathcal{B}(\text{Z} \rightarrow \ell^+\ell^-) = 1.15 \pm 0.01\,(\text{stat.}) \pm 0.02\,(\text{syst.}) \pm 0.03\,(\text{lum.})\,\text{nb}$ for the dilepton mass in the range of 60 to 120 GeV. The measured values agree with next-to-next-to-leading-order QCD cross section calculations. Ratios of cross sections are reported with a precision of 2%. This is the first measurement of inclusive W and Z boson production in proton-proton collisions at $\sqrt{s} = 8\,\text{TeV}$.

[*]See Appendix B for the list of collaboration members

arXiv:1402.0923v2 [hep-ex] 19 May 2014

The production of W and Z bosons is one of the most prominent examples of hard scattering processes at hadron colliders [1]. Theoretical predictions are available at next-to-next-to-leading order (NNLO) [2–6] in perturbative quantum chromodynamics (QCD). The calculations are limited by uncertainties in parton distribution functions (PDFs), missing higher-order QCD effects, and electroweak (EW) radiative corrections, which are available at next-to-leading order (NLO) [7–10]. Precise measurements of inclusive cross sections provide tests of perturbative QCD and validate the theoretical predictions of higher-order corrections. Additionally, accurate measurements can be used to constrain PDFs.

Inclusive W and Z boson production cross sections and their ratios were previously measured by the ATLAS and CMS Collaborations at the Large Hadron Collider (LHC) in proton-proton collisions at $\sqrt{s} = 7$ TeV [11–13]. This Letter describes the inclusive measurement at $\sqrt{s} = 8$ TeV, performed in the electron and muon decay channels, with the CMS detector. A data sample collected in 2012 corresponding to an integrated luminosity of 18.2 ± 0.5 pb^{-1} is used.

The levels of instantaneous luminosity reached by the LHC in 2012 present challenges for the precise measurement of the W boson cross section because of the degraded missing transverse momentum resolution resulting from the large number of pp interactions per bunch crossing (pileup). A data sample with low pileup was collected in May 2012 by adjusting the beam separation during data taking. An average of 4 interactions per bunch crossing was achieved, compared with the average of 21 during the rest of 2012. The measurements of the W and Z boson production cross sections are performed using this data sample.

The central feature of the CMS apparatus is a superconducting solenoid, of 6 m internal diameter, providing a field of 3.8 T. Within the field volume are a silicon pixel and strip tracker, a crystal electromagnetic calorimeter (ECAL), and a brass/scintillator hadron calorimeter. Muons are measured in gas-ionization detectors embedded in the steel flux-return yoke of the magnet. CMS uses a right-handed coordinate system, with the origin at the nominal interaction point, the x axis pointing to the center of the LHC, the y axis pointing upwards, perpendicular to the plane of the LHC ring, and the z axis along the counterclockwise-beam direction. The polar angle θ is measured from the positive z axis, and the azimuthal angle ϕ is measured in the x-y plane. The pseudorapidity η is defined by $\eta = -\ln[\tan(\theta/2)]$. Details of the CMS detector and its performance can be found elsewhere [14].

Leptonic W boson decays are characterized by a prompt, energetic, and isolated charged lepton and a neutrino giving rise to significant missing transverse energy, $E_{\mathrm{T}}^{\mathrm{miss}}$. Events used in the cross section measurement are not required to have a minimum reconstructed $E_{\mathrm{T}}^{\mathrm{miss}}$, but the $E_{\mathrm{T}}^{\mathrm{miss}}$ distribution is used as a discriminant against background from multijet events. Z boson decays to leptons are selected by requiring two energetic and isolated leptons of the same flavor and opposite charge. The Z boson candidates are required to have a reconstructed dilepton mass between 60 and 120 GeV. Samples of Z boson candidates satisfying looser lepton requirements are used to estimate efficiencies.

Because of the high rate of collisions and the limited bandwidth for data processing, the data acquisition system must be selective in deciding which events are sufficiently interesting to be kept for analysis. Triggers make rapid decisions by executing simplified muon and electron reconstruction algorithms. For this analysis, the events are collected when triggered by the presence of a muon with large transverse momentum, $p_{\mathrm{T}} > 15$ GeV, and $|\eta| < 2.1$, or an electron with large transverse energy, $E_{\mathrm{T}} > 22$ GeV, and $|\eta| < 2.5$, with loose isolation and identification requirements.

Electrons are identified as clusters of energy deposits in the ECAL matched to tracks measured

with the silicon tracker [15–19]. The ECAL fiducial region is defined by $|\eta| < 1.44$ (barrel) or $1.57 < |\eta| < 2.5$ (endcap), where η is the pseudorapidity of the energy cluster. The barrel-endcap transition region and the first ring of endcap trigger towers are excluded because they are partially obscured by cables and services exiting between the barrel and endcaps. A cluster is considered to be within the acceptance of the ECAL if it is within the ECAL fiducial region and has transverse energy $E_T > 25\,\mathrm{GeV}$. Electrons are required to be isolated from other reconstructed particles in a cone of $\Delta R = 0.3$, where $\Delta R = \sqrt{\Delta\eta^2 + \Delta\phi^2}$. Particle candidates are identified using a particle-flow algorithm [20, 21] that provides a complete description of the event in terms of electrons, muons, photons, charged hadrons, and neutral hadrons. An electron candidate is selected if the sum of transverse momenta of particles in the cone is less than 15% of the candidate's transverse energy.

Muons are reconstructed from seed tracks in the muon detector combined with silicon strip and pixel information using a global fit [22, 23]. In the p_T range of interest, the momentum resolution is driven by the inner tracking system. Muons with $p_T > 25\,\mathrm{GeV}$ and $|\eta| < 2.1$ are selected, which is consistent with the acceptance of the single muon trigger. A relative isolation variable is computed as discussed for electrons, but in a cone of radius $\Delta R = 0.4$ and with an isolation selection requirement of less than 12%.

The acceptance for W or Z boson events is the fraction of generated events for which the leptons satisfy the restrictions on η and p_T. The event selection criteria will select a subset of the accepted events, and the efficiency specifies the fraction of events selected. This accounts for example for the region of the ECAL from $1.44 < |\eta| < 1.55$. Other effects, like crystal boundaries, are accounted in the efficiency to reconstruct leptons. Using this acceptance definition, we are able to separate experimental from theoretical uncertainties in the measurement. The detector response is simulated using a detailed description of the CMS detector, based on the GEANT4 package [24]. Additional proton-proton interactions are taken into account using an admixture of simulated minimum bias events and the same reconstruction code is applied for data and simulated events. Data to simulation ratios of efficiencies are used as scale factors. No single event generator gives a reliable description of both EW and QCD effects. The acceptance is estimated using Monte Carlo simulation based on POWHEG [25–28]. The effects of nonperturbative QCD, higher-order QCD, and electroweak corrections on the estimated acceptance are investigated using specific simulation tools, from which uncertainties are derived [7–10, 29, 30]. The uncertainty related to the PDFs is estimated following closely the prescription of the PDF4LHC working group [31] to combine uncertainties related to the choice of the NLO PDF and the strong coupling constant, α_s.

The W boson candidate events are required to have an identified electron or muon. The W boson signal and background yields are obtained from the E_T^{miss} distributions using a binned maximum-likelihood fit. The missing transverse energy is calculated with the particle-flow algorithm by adding the transverse energy vectors of all identified particles. An accurate E_T^{miss} measurement is essential to distinguish the W signal from QCD multijet backgrounds. To account for shortcomings of the simulation in modeling the recoil against the W boson, a correction is derived from a Z boson sample. The recoil in these events is studied, in data as well as in simulation, and the differences are propagated to the W boson simulation as a function of the p_T of the generated W or Z boson. Other background processes from $W \to \tau\nu$, Drell–Yan, diboson, and top-pair production also become significant at high E_T^{miss}, contributing about 6% of the total selected yield. The background contribution from cosmic rays in the $W \to \mu\nu$ channel is negligible. The E_T^{miss} model is fitted to the observed distribution as the sum of three contributions: the W signal, the QCD background, and other backgrounds. The QCD background is modeled by an analytic function, while the signal and EW backgrounds are modeled with

simulation-based fitting functions [11]. The EW contributions are normalized to the W signal yield in the fit through the ratios of the theoretical cross sections. Figure 1 shows the E_T^{miss} distributions of the inclusive W boson samples and the results of the fit.

To extract the Z boson yield, the events in the dilepton mass window are counted. The yields contain a contribution of 3% from γ^*-mediated processes, including interference effects, as estimated with MCFM [32]. Background contamination is estimated from simulation to be about 0.4%. Figure 2 shows the dilepton mass distributions of the inclusive Z samples. The signal yields, the acceptances, and the efficiencies are summarized in Appendix A.
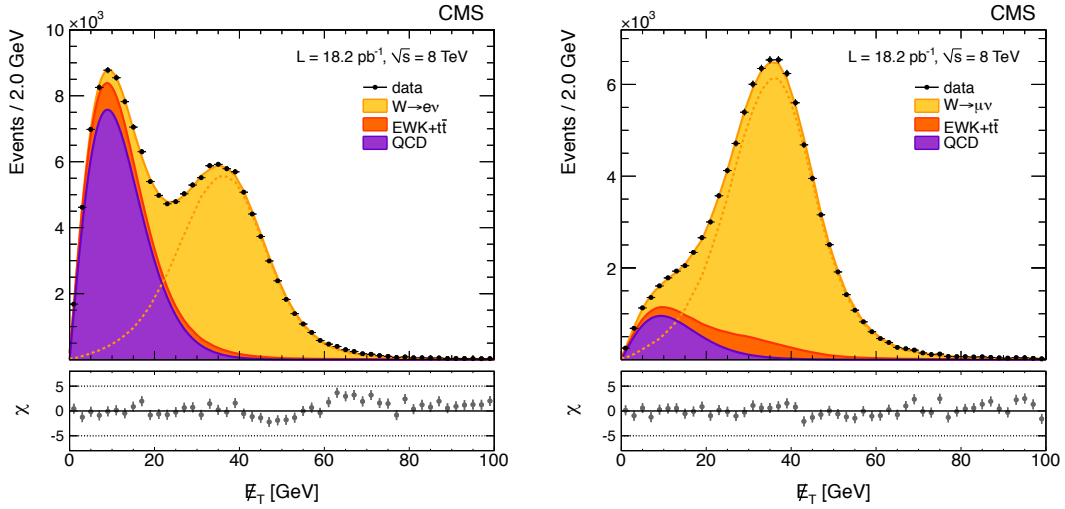

Figure 1: The missing transverse energy distributions for W boson candidate events in the electron (left) and muon (right) final states. The variable χ shown in the lower plot is defined as $(N_{obs} - N_{exp})/\sqrt{N_{obs}}$, where N_{obs} is the number of observed events and N_{exp} is the total of the fitted signal and background yields.

The systematic uncertainties are summarized in Table 1 for the electron and muon channels. The methods used to extract the systematic uncertainties for the acceptance, efficiency, and signal extraction follow closely the W and Z boson cross section measurements performed at $\sqrt{s} = 7\,\text{TeV}$ [11]. The leading experimental uncertainty comes from the measurement of the lepton reconstruction and identification efficiency. Other uncertainties come from the integrated luminosity of the data sample and theoretical uncertainties, which are dominated by the PDF uncertainties.

The luminosity of the data sample is measured with an uncertainty of 2.6% by counting the number of clusters per event in the silicon pixel detector. The highly granular detector, consisting of ~60 million channels, guarantees an excellent linearity of the pixel detector response versus pileup. The method is calibrated by means of a procedure pioneered by van der Meer [39], consisting of beam scans along the vertical and horizontal directions. This van der Meer technique determines the luminosity at the percent level from a measurement of the beam parameters [40]. The dominant contribution to the luminosity uncertainty originates from the assumptions on the functional form of the beam shapes.

The theoretical predictions of cross sections and cross section ratios are computed at NNLO with the program FEWZ [41] and the MSTW2008 [42] set of PDFs. The uncertainties in these predictions, at the 68% confidence level (CL), include contributions from the uncertainty of the strong coupling constant α_s [43, 44], the choice of heavy-quark masses (charm and bottom
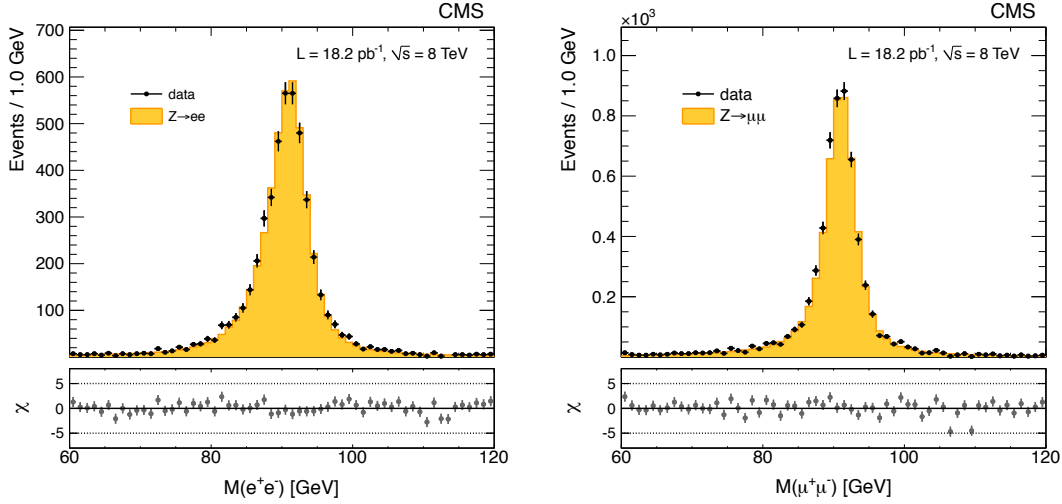
Figure 2: The dilepton mass distributions for Z boson candidate events in the electron (left) and muon (right) final states. The variable χ shown in the lower plot is defined as $(N_{obs} - N_{exp})/\sqrt{N_{obs}}$, where N_{obs} is the number of observed events and N_{exp} is the total of the signal and background yields.

Table 1: Systematic uncertainties in percent for the electron and muon channels; "—" means that the source either does not apply or is negligible.

Sources	W^+		W^-		W		W^+/W^-		Z		W/Z	
	e	μ	e	μ	e	μ	e	μ	e	μ	e	μ
Lepton reconstruction & identification	2.8	1.0	2.5	0.9	2.5	1.0	3.8	1.2	2.8	1.1	3.8	1.5
Momentum scale & resolution	0.4	0.3	0.7	0.3	0.5	0.3	0.3	0.1	—	—	0.5	0.3
E_T^{miss} scale & resolution	0.8	0.5	0.7	0.5	0.8	0.5	0.3	0.1	—	—	0.8	0.5
Background subtraction / modeling	0.2	0.2	0.3	0.1	0.3	0.1	0.1	0.2	0.4	0.4	0.5	0.4
Total experimental	3.0	1.2	2.7	1.1	2.7	1.2	3.8	1.2	2.8	1.2	3.9	1.7
Theoretical uncertainty	2.1	2.0	2.6	2.5	2.7	2.2	1.5	1.4	2.6	1.9	2.0	2.5
Luminosity	2.6	2.6	2.6	2.6	2.6	2.6	—	—	2.6	2.6	—	—
Total	4.5	3.5	4.6	3.8	4.6	3.6	4.1	1.8	4.6	3.4	4.4	3.0

quarks) [45], as well as neglected higher-order corrections beyond NNLO, which are estimated by allowing the renormalization and factorization scales to vary. The NNLO predictions for the total cross sections times branching fractions are 7.12 ± 0.20 nb for W^+, 5.06 ± 0.13 nb for W^-, and 1.13 ± 0.04 nb for Z boson production. The Z boson cross section requires an invariant mass within the range 60 to 120 GeV, and it includes the effects of virtual photons.

The results in the electron and muon decay channels are compatible with a p-value of 0.42. Assuming universality of lepton couplings to W and Z bosons, the channels are combined by calculating an average cross section value weighted by their statistical and systematic uncertainties, taking into account the correlated uncertainties. The two leptonic decay channels are combined by assuming fully correlated uncertainties for the acceptance and luminosity, but with other uncertainties assumed to be uncorrelated.

In measurements of the ratios of cross sections some systematic uncertainties cancel, most importantly the uncertainty in the luminosity. The uncertainties in the lepton reconstruction and identification are treated as uncorrelated and the resulting experimental uncertainty in the ratio measurements can therefore be larger than for individual cross section measurements. A summary of the measurements is given in Table 2, including the results obtained within the fiducial

Table 2: Summary of total and fiducial W^+, W^-, W, and Z production cross sections times branching fractions, W to Z and W^+ to W^- ratios, and their theoretical predictions.

Channel	$\sigma \times \mathcal{B}$ [nb] (total)	NNLO [nb]	Quantity	Ratio (total)	NNLO
W^+	$7.11 \pm 0.03\,(\text{stat.}) \pm 0.14\,(\text{syst.}) \pm 0.18\,(\text{lum.})$	7.12 ± 0.20	R_{W^+/W^-}	$1.39 \pm 0.01\,(\text{stat.}) \pm 0.02\,(\text{syst.})$	1.41 ± 0.01
W^-	$5.09 \pm 0.02\,(\text{stat.}) \pm 0.11\,(\text{syst.}) \pm 0.13\,(\text{lum.})$	5.06 ± 0.13	$R_{W/Z}$	$10.63 \pm 0.11\,(\text{stat.}) \pm 0.25\,(\text{syst.})$	10.74 ± 0.04
W	$12.21 \pm 0.03\,(\text{stat.}) \pm 0.24\,(\text{syst.}) \pm 0.32\,(\text{lum.})$	12.18 ± 0.32			
Z	$1.15 \pm 0.01\,(\text{stat.}) \pm 0.02\,(\text{syst.}) \pm 0.03\,(\text{lum.})$	1.13 ± 0.04			
Channel	$\sigma \times \mathcal{B}$ [nb] (fiducial)	NNLO [nb]	Quantity	Ratio (fiducial)	NNLO
W^+	$3.16 \pm 0.01\,(\text{stat.}) \pm 0.04\,(\text{syst.}) \pm 0.08\,(\text{lum.})$	3.18 ± 0.10	R_{W^+/W^-}	$1.40 \pm 0.01\,(\text{stat.}) \pm 0.02\,(\text{syst.})$	1.42 ± 0.02
W^-	$2.26 \pm 0.01\,(\text{stat.}) \pm 0.02\,(\text{syst.}) \pm 0.06\,(\text{lum.})$	2.25 ± 0.07	$R_{W/Z}$	$13.26 \pm 0.15\,(\text{stat.}) \pm 0.21\,(\text{syst.})$	13.49 ± 0.28
W	$5.42 \pm 0.02\,(\text{stat.}) \pm 0.06\,(\text{syst.}) \pm 0.14\,(\text{lum.})$	5.43 ± 0.16			
Z	$0.41 \pm 0.01\,(\text{stat.}) \pm 0.01\,(\text{syst.}) \pm 0.01\,(\text{lum.})$	0.40 ± 0.01			

regions in p_T and η. See Appendix A for the total cross sections times branching fractions and ratios for the electron and muon decay channels.

The upper two plots in Fig. 3 show the measured and predicted W versus Z and W^+ versus W^- cross sections for different PDF sets. The uncertainties in the theoretical predictions correspond to the PDF uncertainties only. This approach eliminates the need to propagate acceptance uncertainties originating from the PDFs and higher-order corrections into the measurement. The final measurement is compared with the predicted cross sections in the acceptance region for three different PDFs with their respective uncertainty bands propagated through the prediction.

In summary, we have performed the first measurements of total and fiducial inclusive W and Z production cross sections times branching fractions in pp collisions at $\sqrt{s} = 8\,\text{TeV}$ using $18.2 \pm 0.5\,\text{pb}^{-1}$ of low-pileup data recorded with the CMS detector. The W and Z bosons are observed via their decays to electrons and muons. The measured total inclusive production cross sections times branching fractions are $\sigma(\text{pp} \rightarrow WX) \times \mathcal{B}(W \rightarrow \ell\nu) = 12.21 \pm 0.03\,(\text{stat.}) \pm 0.24\,(\text{syst.}) \pm 0.32\,(\text{lum.})\,\text{nb}$ and, for the dilepton mass in the range of 60 to 120 GeV, $\sigma(\text{pp} \rightarrow ZX) \times \mathcal{B}(Z \rightarrow \ell^+\ell^-) = 1.15 \pm 0.01\,(\text{stat.}) \pm 0.02\,(\text{syst.}) \pm 0.03\,(\text{lum.})\,\text{nb}$. In addition to the inclusive cross sections, we present ratios of cross sections measured with a precision of 2%. The measurements in the electron and muon channels are consistent, and in agreement with NNLO calculations. Additional figures summarizing our measurements are available in Appendix A.
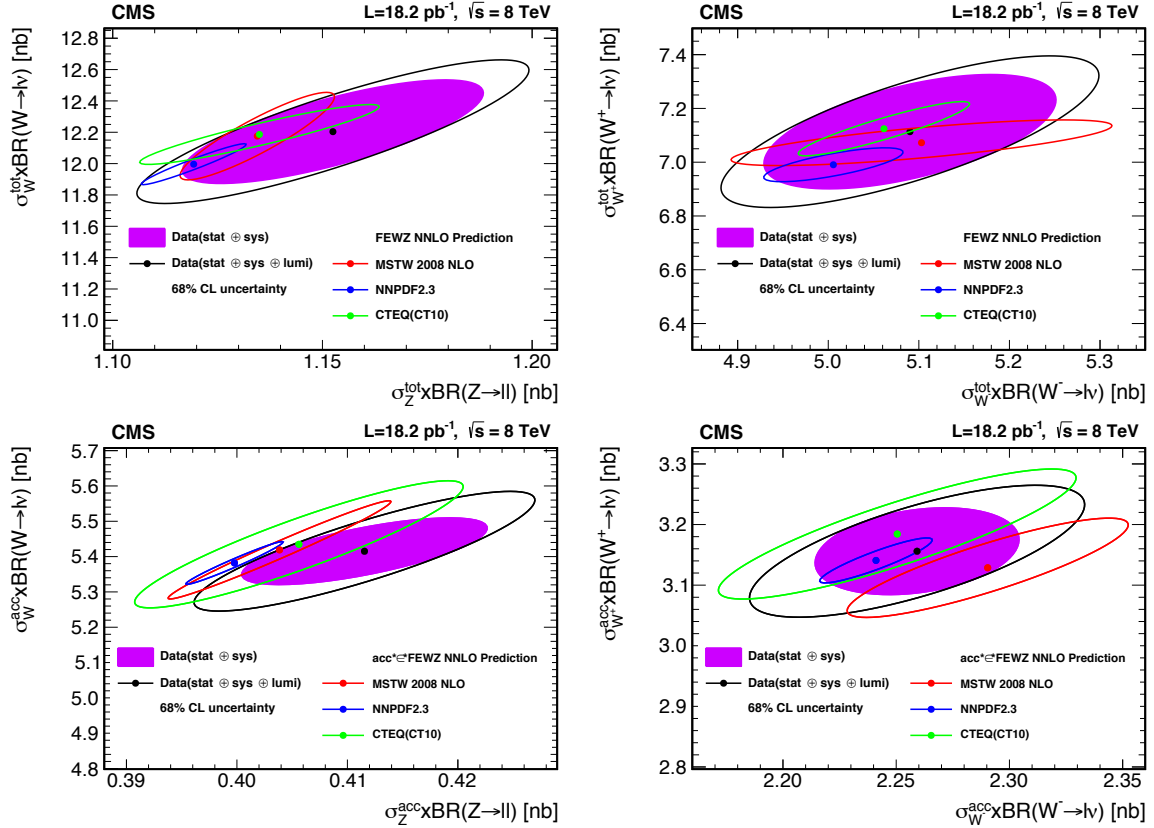
Figure 3: Measured and predicted W versus Z boson (left column) and W^+ versus W^- boson (right column) production cross sections times branching fractions. The ellipses illustrate the 68% CL coverage for total uncertainties (open) and excluding the luminosity uncertainty (filled). The top row shows the inclusive cross sections times branching fractions and the bottom row shows the results within the fiducial regions. The uncertainties in the theoretical predictions correspond to the PDF uncertainty components only and are evaluated for MSTW 2008 NLO [42], NNPDF 2.3 [46], and CT10 [47].

References

[1] S. D. Drell and T.-M. Yan, "Massive Lepton-Pair Production in Hadron-Hadron Collisions at High Energies", *Phys. Rev. Lett.* **25** (1970) 316, `doi:10.1103/PhysRevLett.25.316`.

[2] P. J. Rijken and W. L. van Neerven, "Order α_s^2 contributions to the Drell-Yan cross section at fixed target energies", *Phys. Rev. D* **51** (1995) 44, `doi:10.1103/PhysRevD.51.44`.

[3] R. Hamberg, W. L. van Neerven, and T. Matsuura, "A complete calculation of the order α_s^2 correction to the Drell-Yan K-factor", *Nucl. Phys. B* **359** (1991) 343, `doi:10.1016/0550-3213(91)90064-5`.

[4] W. L. van Neerven and E. B. Zijlstra, "The $O(\alpha_s^2)$ corrected Drell-Yan K-factor in the DIS and $\overline{\text{MS}}$ schemes", *Nucl. Phys. B* **382** (1992) 11, `doi:10.1016/0550-3213(92)90078-P`.

[5] R. V. Harlander and W. B. Kilgore, "Next-to-Next-to-Leading Order Higgs Production at Hadron Colliders", *Phys. Rev. Lett.* **88** (2002) 201801, `doi:10.1103/PhysRevLett.88.201801`.

[6] C. Anastasiou, L. Dixon, K. Melnikov, and F. Petriello, "High-precision QCD at hadron colliders: Electroweak gauge boson rapidity distributions at next-to-next-to-leading order", *Phys. Rev. D* **69** (2004) 094008, `doi:10.1103/PhysRevD.69.094008`.

[7] C. M. Carloni Calame, G. Montagna, O. Nicrosini, and A. Vicini, "Precision electroweak calculation of the production of a high transverse-momentum lepton pair at hadron colliders", *J. High Energy Phys.* **10** (2007) 109, `doi:10.1088/1126-6708/2007/10/109`.

[8] C. M. Carloni Calame, G. Montagna, O. Nicrosini, and A. Vicini, "Precision electroweak calculation of the charged current Drell–Yan process", *J. High Energy Phys.* **12** (2006) 16, `doi:10.1088/1126-6708/2006/12/016`.

[9] C. M. Carloni Calame, G. Montagna, O. Nicrosini, and M. Treccani, "Multiple photon corrections to the neutral-current Drell-Yan process", *J. High Energy Phys.* **05** (2005) 019, `doi:10.1088/1126-6708/2005/05/019`.

[10] C. M. Carloni Calame, G. Montagna, O. Nicrosini, and M. Treccani, "Higher-order QED corrections to *W*-boson mass determination at hadron colliders", *Phys. Rev. D* **69** (2004) 037301, `doi:10.1103/PhysRevD.69.037301`.

[11] CMS Collaboration, "Measurement of the inclusive W and Z production cross sections in pp collisions at $\sqrt{s} = 7$ TeV with the CMS experiment", *J. High Energy Phys.* **10** (2011) 132, `doi:10.1007/JHEP10(2011)132`.

[12] CMS Collaboration, "Measurement of the inclusive Z cross section via decays to tau pairs in pp collisions at $\sqrt{s} = 7$ TeV", *J. High Energy Phys.* **08** (2011) 117, `doi:10.1007/JHEP08(2011)117`.

[13] ATLAS Collaboration, "Measurement of the inclusive $W^{\pm}$ and $Z/\gamma*$ cross sections in the *e* and *μ* decay channels in *pp* collisions $\sqrt{s} = 7$ TeV with the ATLAS detector", *Phys. Rev. D* **85** (2012) 072004, `doi:10.1103/PhysRevD.85.072004`.

[14] CMS Collaboration, "The CMS experiment at the CERN LHC", *JINST* **3** (2008) S08004, `doi:10.1088/1748-0221/3/08/S08004`.

[15] W. Adam, R. Frühwirth, A. Strandlie, and T. Todor, "Reconstruction of Electrons with the Gaussian-Sum Filter in the CMS Tracker at the LHC", Technical Report CMS-NOTE-2005-001, 2005.

[16] CMS Collaboration, "CMS tracking performance results from early LHC operation", *Eur. Phys. J. C* **70** (2010) 1165, `doi:10.1140/epjc/s10052-010-1491-3`.

[17] CMS Collaboration, "Energy calibration and resolution of the CMS electromagnetic calorimeter in pp collisions at $\sqrt{s} = 7$ TeV", *JINST* **8** (2013) P09009, `doi:10.1088/1748-0221/8/09/P09009`, `arXiv:1306.2016`.

[18] CMS Collaboration, "Measurement of the Isolated Prompt Photon Production Cross Section in pp Collisions at $\sqrt{s} = 7$ TeV", *Phys. Rev. Lett.* **106** (2011) 082001, `doi:10.1103/PhysRevLett.106.082001`.

[19] S. Baffioni et al., "Electron reconstruction in CMS", *Eur. Phys. J. C* **49** (2007) 1099, `doi:10.1140/epjc/s10052-006-0175-5`.

[20] CMS Collaboration, "Commissioning of the Particle-flow Event Reconstruction with the first LHC collisions recorded in the CMS detector", CMS Physics Analysis Summary CMS-PAS-PFT-10-001, 2010.

[21] CMS Collaboration, "Commissioning of the particle-flow event reconstruction with leptons from J/Ψ and W decays at 7 TeV", CMS Physics Analysis Summary CMS-PAS-PFT-10-003, 2010.

[22] CMS Collaboration, "Performance of muon identification in pp collisions at $\sqrt{s}$ = 7 TeV", CMS Physics Analysis Summary CMS-PAS-MUO-10-002, 2010.

[23] CMS Collaboration, "Performance of CMS muon reconstruction in cosmic-ray events", *JINST* **5** (2010) T03022, `doi:10.1088/1748-0221/5/03/T03022`.

[24] GEANT4 Collaboration, "GEANT4—a simulation toolkit", *Nucl. Instrum. Meth. A* **506** (2003) 250, `doi:10.1016/S0168-9002(03)01368-8`.

[25] S. Alioli, P. Nason, C. Oleari, and E. Re, "NLO Vector Boson Production Matched with Shower in POWHEG", *J. High Energy Phys.* **07** (2008) 060, `doi:10.1088/1126-6708/2008/07/060`.

[26] P. Nason, "A New Method for Combining NLO QCD with Shower Monte Carlo Algorithms", *J. High Energy Phys.* **11** (2004) 040, `doi:10.1088/1126-6708/2004/11/040`.

[27] S. Frixione, P. Nason, C. Oleari, "Matching NLO QCD computations with parton shower simulations: the POWHEG method", *J. High Energy Phys.* **11** (2007) 070, `doi:10.1088/1126-6708/2007/11/070`.

[28] S. Alioli, P. Nason, C. Oleari, and E. Re, "A General Framework for Implementing NLO Calculations in Shower Monte Carlo Programs: the POWHEG BOX", *J. High Energy Phys.* **06** (2010) 043, `doi:10.1007/JHEP06(2010)043`.

[29] C. Balázs and C.-P. Yuan, "Soft gluon effects on lepton pairs at hadron colliders", *Phys. Rev. D* **56** (1997) 5558, `doi:10.1103/PhysRevD.56.5558`.

[30] E. Barberio, B. van Eijk, and Z. Wąs, "Photos — a universal Monte Carlo for QED radiative corrections in decays", *Comp. Phys. Commun.* **66** (1991) 115, `doi:10.1016/0010-4655(91)90012-A`.

[31] M. Botje et al., "The PDF4LHC Working Group Interim Recommendations", (2011). `arXiv:1101.0538`.

[32] J. M. Campbell and R. K. Ellis, "MCFM for the Tevatron and the LHC", *Nucl. Phys. Proc. Suppl.* **205** (2010) 10, `doi:10.1016/j.nuclphysbps.2010.08.011`, `arXiv:1007.3492`.

[33] UA1 Collaboration, "Intermediate Vector Boson Cross-sections at the CERN Super Proton Synchrotron Collider and the Number of Neutrino Types", *Phys. Lett. B* **198** (1987) 271, `doi:10.1016/0370-2693(87)91510-3`.

[34] UA2 Collaboration, "A Measurement of the W and Z Production Cross-sections and a Determination of Γ_W at the CERN $\overline{p}p$ collider", *Phys. Lett. B* **276** (1992) 365, doi:10.1016/0370-2693(92)90333-Y.

[35] CDF Collaboration, "Measurement of $\sigma \times B(W \to e\nu)$ and $\sigma \times B(Z \to e^+e-)$ in $p\overline{p}$ collisions at $\sqrt{s} = 1.8$ TeV ", *Phys. Rev. Lett.* **76** (1996) 3070, doi:10.1103/PhysRevLett.76.3070.

[36] CDF Collaboration, "Measurement of Z^0 and Drell-Yan production cross section using dimuons in $\overline{p}p$ collisions at $\sqrt{s} = 1.8$ TeV ", *Phys. Rev. D* **59** (1999) 052002, doi:10.1103/PhysRevD.59.052002.

[37] CDF Collaboration, "Measurements of Inclusive W and Z Cross-sections in $p\overline{p}$ Collisions at $\sqrt{s} = 1.96$ TeV ", *J. Phys. G* **34** (2007) 2457, doi:10.1088/0954-3899/34/12/001.

[38] D0 Collaboration, "Extraction of the width of the W boson from measurements of $\sigma(p\overline{p} \to W + X) \times B(W \to e\nu)$ and $\sigma(p\overline{p} \to Z + X) \times B(Z \to ee)$ and their ratio", *Phys. Rev. D* **61** (2000) 072001, doi:10.1103/PhysRevD.61.072001.

[39] S. van der Meer, "Calibration of the effective beam height in the ISR", Technical Report CERN-ISR-PO-68-31. ISR-PO-68-31, 1968.

[40] CMS Collaboration, "CMS Luminosity Based on Pixel Cluster Counting - Summer 2012 Update", CMS Physics Analysis Summary CMS-PAS-LUM-12-001, 2012.

[41] K. Melnikov and F. Petriello, "W Boson Production Cross Section at the Large Hadron Collider with $\mathcal{O}(\alpha^2)$ Corrections", *Phys. Rev. Lett.* **96** (2006) 231803, doi:10.1103/PhysRevLett.96.231803.

[42] A. D. Martin, W. J. Stirling, R. S. Thorne, and G. Watt, "Parton distributions for the LHC", *Eur. Phys. J. C* **63** (2009) 189, doi:10.1140/epjc/s10052-009-1072-5.

[43] A. Martin, W. Stirling, R. Thorne, and G. Watt, "Uncertainties on α_s in global PDF analyses and implications for predicted hadronic cross sections", *Eur. Phys. J. C* **64** (2009) 653, doi:10.1140/epjc/s10052-009-1164-2.

[44] G. Watt, "Parton distribution function dependence of benchmark Standard Model total cross sections at the 7 TeV LHC", *J. High Energy Phys.* **09** (2011) 069, doi:10.1007/JHEP09(2011)069.

[45] A. Martin, W. Stirling, R. Thorne, and G. Watt, "Heavy-quark mass dependence in global PDF analyses and 3- and 4-flavour parton distributions", *Eur. Phys. J. C* **70** (2010) 51, doi:10.1140/epjc/s10052-010-1462-8.

[46] R. D. Ball et al., "Parton distributions with LHC data", *Nucl. Phys. B* **867** (2013) 244, doi:10.1016/j.nuclphysb.2012.10.003.

[47] H.-L. Lai et al., "New parton distributions for collider physics", *Phys. Rev. D* **82** (2010) 074024, doi:10.1103/PhysRevD.82.074024.

A   Total cross sections times branching fractions and ratios for the electron and muon decay channels

Table 3: The signal yields, acceptances, and efficiencies. The Z boson yield uncertainties are given by Poisson statistics, while the W boson yield uncertainties are determined from the fit. Uncertainties in the acceptances and efficiencies are systematic uncertainties.

Source	$Z \to e^+e^-$	$W \to e\nu$	$W^+ \to e^+\nu$	$W^- \to e^-\bar{\nu}$
Yields	4793 ± 69	75051 ± 287	44194 ± 219	30857 ± 185
Acceptance	0.399 ± 0.010	0.479 ± 0.013	0.484 ± 0.011	0.471 ± 0.013
Efficiency	0.585 ± 0.016	0.695 ± 0.019	0.687 ± 0.021	0.708 ± 0.019
Source	$Z \to \mu^+\mu^-$	$W \to \mu\nu$	$W^+ \to \mu^+\nu$	$W^- \to \mu^-\bar{\nu}$
Yields	5917 ± 77	81473 ± 282	47637 ± 216	33836 ± 182
Acceptance	0.346 ± 0.007	0.440 ± 0.010	0.441 ± 0.009	0.439 ± 0.011
Efficiency	0.809 ± 0.010	0.839 ± 0.010	0.843 ± 0.010	0.831 ± 0.009

Table 4:   Summary of total W^+, W^-, W, and Z production cross sections times branching fractions, W to Z and W^+ to W^- ratios, and their theoretical predictions.

Channel		$\sigma \times \mathcal{B}$ [nb] (total)	NNLO [nb]
	$e^+\nu$	$7.31 \pm 0.04\,\text{(stat.)} \pm 0.26\,\text{(syst.)} \pm 0.19\,\text{(lum.)}$	
W^+	$\mu^+\nu$	$7.04 \pm 0.03\,\text{(stat.)} \pm 0.16\,\text{(syst.)} \pm 0.18\,\text{(lum.)}$	7.12 ± 0.20
	$\ell^+\nu$	$7.11 \pm 0.03\,\text{(stat.)} \pm 0.14\,\text{(syst.)} \pm 0.18\,\text{(lum.)}$	
	$e^-\nu$	$5.08 \pm 0.03\,\text{(stat.)} \pm 0.19\,\text{(syst.)} \pm 0.13\,\text{(lum.)}$	
W^-	$\mu^-\nu$	$5.09 \pm 0.03\,\text{(stat.)} \pm 0.14\,\text{(syst.)} \pm 0.13\,\text{(lum.)}$	5.06 ± 0.13
	$\ell^-\nu$	$5.09 \pm 0.02\,\text{(stat.)} \pm 0.11\,\text{(syst.)} \pm 0.13\,\text{(lum.)}$	
	$e\nu$	$12.39 \pm 0.05\,\text{(stat.)} \pm 0.44\,\text{(syst.)} \pm 0.32\,\text{(lum.)}$	
W	$\mu\nu$	$12.13 \pm 0.04\,\text{(stat.)} \pm 0.29\,\text{(syst.)} \pm 0.32\,\text{(lum.)}$	12.18 ± 0.32
	$\ell\nu$	$12.21 \pm 0.03\,\text{(stat.)} \pm 0.24\,\text{(syst.)} \pm 0.32\,\text{(lum.)}$	
	e^+e^-	$1.13 \pm 0.02\,\text{(stat.)} \pm 0.05\,\text{(syst.)} \pm 0.03\,\text{(lum.)}$	
Z	$\mu^+\mu^-$	$1.16 \pm 0.02\,\text{(stat.)} \pm 0.03\,\text{(syst.)} \pm 0.03\,\text{(lum.)}$	1.13 ± 0.04
	$\ell^+\ell^-$	$1.15 \pm 0.01\,\text{(stat.)} \pm 0.02\,\text{(syst.)} \pm 0.03\,\text{(lum.)}$	
Quantity		Ratio (total)	NNLO
	e	$1.44 \pm 0.01\,\text{(stat.)} \pm 0.05\,\text{(syst.)}$	
R_{W^+/W^-}	μ	$1.38 \pm 0.01\,\text{(stat.)} \pm 0.03\,\text{(syst.)}$	1.41 ± 0.01
	ℓ	$1.39 \pm 0.01\,\text{(stat.)} \pm 0.02\,\text{(syst.)}$	
	e	$10.99 \pm 0.16\,\text{(stat.)} \pm 0.43\,\text{(syst.)}$	
$R_{W/Z}$	μ	$10.44 \pm 0.14\,\text{(stat.)} \pm 0.30\,\text{(syst.)}$	10.74 ± 0.04
	ℓ	$10.63 \pm 0.11\,\text{(stat.)} \pm 0.25\,\text{(syst.)}$	

Table 5: Summary of fiducial inclusive W$^+$, W$^-$, W, and Z production cross sections times branching fractions, W to Z and W$^+$ to W$^-$ ratios, and their theoretical predictions.

| Channel		$\sigma \times \mathcal{B}$ [nb] (total)	NNLO [nb]
	e$^+\nu$	3.54 ± 0.02 (stat.) ± 0.11 (syst.) ± 0.09 (lum.)	3.45 ± 0.12
W$^+$	$\mu^+\nu$	3.10 ± 0.01 (stat.) ± 0.04 (syst.) ± 0.08 (lum.)	3.14 ± 0.11
	$\ell^+\nu$	3.16 ± 0.01 (stat.) ± 0.04 (syst.) ± 0.08 (lum.)	3.18 ± 0.10
	e$^-\nu$	2.39 ± 0.01 (stat.) ± 0.06 (syst.) ± 0.06 (lum.)	2.38 ± 0.09
W$^-$	$\mu^-\nu$	2.24 ± 0.01 (stat.) ± 0.02 (syst.) ± 0.06 (lum.)	2.22 ± 0.08
	$\ell^-\nu$	2.26 ± 0.01 (stat.) ± 0.02 (syst.) ± 0.06 (lum.)	2.25 ± 0.07
	eν	5.94 ± 0.02 (stat.) ± 0.16 (syst.) ± 0.15 (lum.)	5.84 ± 0.22
W	$\mu\nu$	5.34 ± 0.02 (stat.) ± 0.06 (syst.) ± 0.14 (lum.)	5.36 ± 0.18
	$\ell\nu$	5.42 ± 0.02 (stat.) ± 0.06 (syst.) ± 0.14 (lum.)	5.43 ± 0.16
	e$^+$e$^-$	0.45 ± 0.01 (stat.) ± 0.01 (syst.) ± 0.01 (lum.)	0.45 ± 0.02
Z	$\mu^+\mu^-$	0.40 ± 0.01 (stat.) ± 0.01 (syst.) ± 0.01 (lum.)	0.39 ± 0.02
	$\ell^+\ell^-$	0.41 ± 0.01 (stat.) ± 0.01 (syst.) ± 0.01 (lum.)	0.40 ± 0.01
Quantity		Ratio (total)	NNLO
	e	1.48 ± 0.01 (stat.) ± 0.06 (syst.)	1.45 ± 0.02
R_{W^+/W^-}	μ	1.39 ± 0.01 (stat.) ± 0.02 (syst.)	1.41 ± 0.02
	ℓ	1.40 ± 0.01 (stat.) ± 0.02 (syst.)	1.42 ± 0.02
	e	13.19 ± 0.20 (stat.) ± 0.51 (syst.)	12.89 ± 0.26
$R_{W/Z}$	μ	13.28 ± 0.18 (stat.) ± 0.23 (syst.)	13.65 ± 0.35
	ℓ	13.26 ± 0.15 (stat.) ± 0.21 (syst.)	13.49 ± 0.28
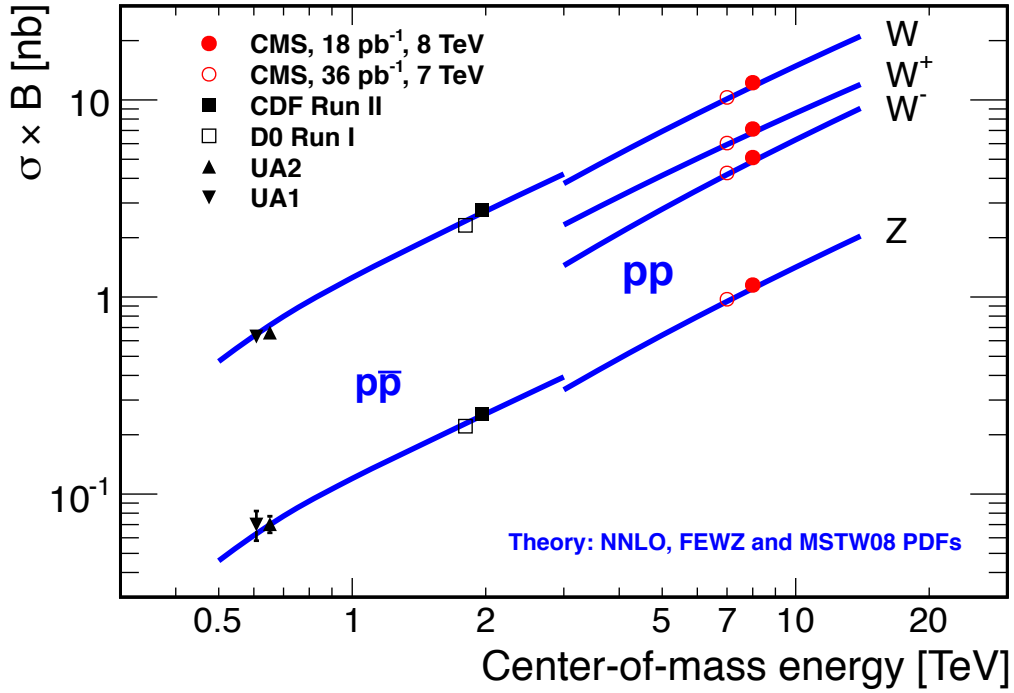
Figure 4: Measurements of the total W$^+$, W$^-$, W, and Z production cross sections times branching fractions versus center-of-mass energy for CMS and experiments at lower-energy colliders [33–38]. The predicted increase of the cross sections with center-of-mass energy is confirmed by our measurements.
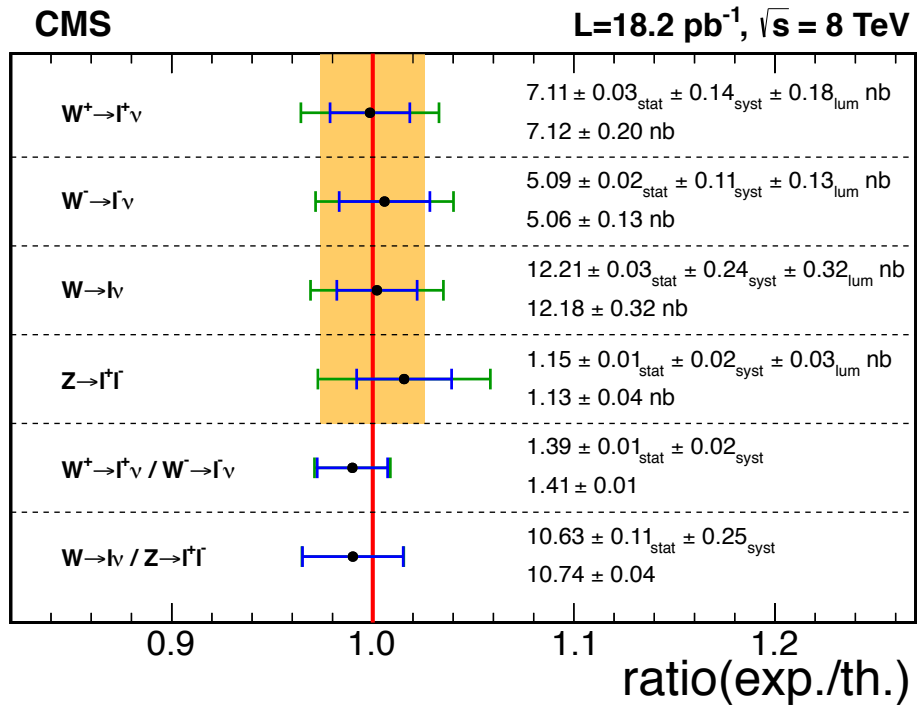
Figure 5: Summary of total inclusive W^+, W^-, W, and Z production cross sections times branching fractions, W to Z and W^+ to W^- ratios, and their theoretical predictions. The shaded box indicates the uncertainties in the luminosity measurement. The inner error bars represent the experimental uncertainties, while outer error bars also include the uncertainties in the theoretical predictions. The individual measurements and theoretical predictions are given numerically on the right.
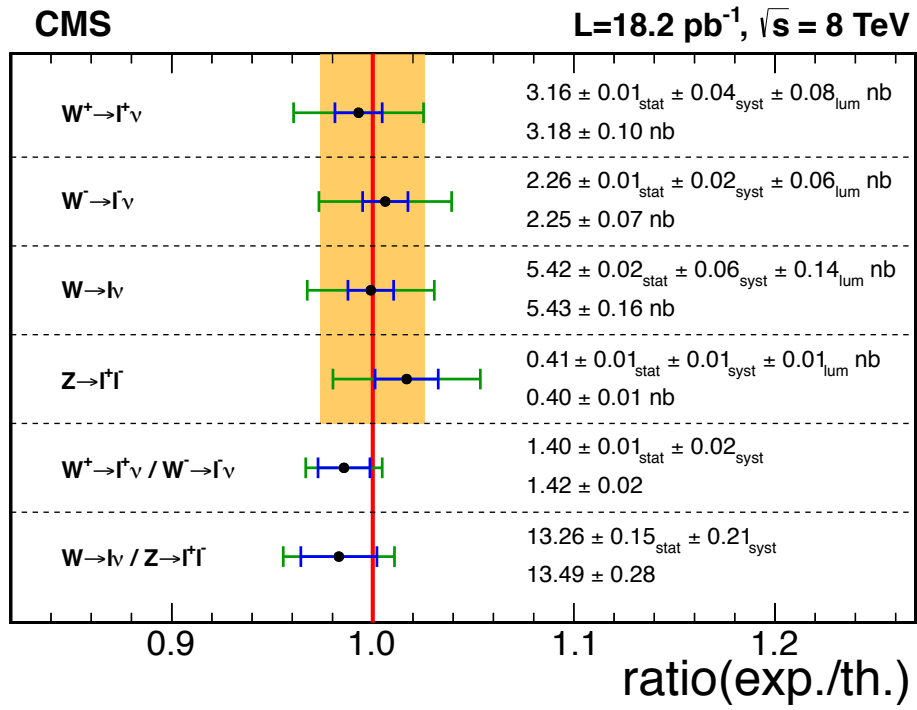
Figure 6: Summary of fiducial inclusive W$^+$, W$^-$, W, and Z production cross sections times branching fractions, W to Z and W$^+$ to W$^-$ ratios, and their theoretical predictions. The shaded box indicates the uncertainties in the luminosity measurement. The inner error bars represent the experimental uncertainties, while outer error bars also include the uncertainties in the theoretical predictions. The individual measurements and theoretical predictions are given numerically on the right.